N85-25866

CRACK ELEMENTS FOR COSMIC/NASTRAN

P. J. Wojtowitz and R. L. Citerley
Anamet Laboratories, Inc., San Carlos, CA 94070

SUMMARY

A new crack element has been developed and incorporated into COSMIC/NASTRAN. The element is considered linear, isotropic, and homogeneous. Mode I and II stress intensity factors are automatically calculated. Comparisons to theoretical plane strain solutions for several geometries are presented and demonstrate the accuracy of the developed element. Extensions of the element to three dimensions, anisotropic material, and plastic analysis are discussed.

INTRODUCTION

Crack or singular elements have been developed for finite element analysis for almost as long as finite element codes have been available. These elements usually are classified as either hybrid or singular element formulations. Many of the elements developed suffered from either lack of accuracy, generality, or consistency. Barsoum (Ref. 1) points out shortcomings of several different elements. These shortcomings include inability to model rigid body or constant strain modes, inability to include thermal or body force effects, and lack of compatibility with other elements.

The elements developed by Barsoum (Ref. 1) and Henshell (Ref. 2) rectified many of the problems described above; however, these elements were limited to displacement of the form $r^{1/2}$. Consequently, they could only model strain singularities of the form $r^{-1/2}$. Recently, Stern (Ref. 3) and more recently, Hughes and Aikin (Ref. 4) have introduced families of consistent, conforming elements which allow displacements of the form r^{γ}. While the Stern element appears to have the restriction that $0 < \gamma < 1$, the element of Hughes and Aikin is valid for all $\gamma > 0$. The element described herein is based upon shape functions suggested by Hughes and Aikin (Ref. 4).

The element presented here possesses the required rigid body and constant strain modes. It properly models thermal, body force, and pressure loading conditions. Additionally, it is compatible with standard linear or quadratic isoparametric elements and can possess either 5 or 6 nodes. Finally, it can be used as a nonsingular element with a variable number of nodes.

ELEMENT FORMULATION

The following derivation follows Hughes and Aikin (Ref. 4). Referring to Figure 1, the standard bilinear shape functions are used for nodes 1 through 4:

$$\begin{aligned} N_1(r,s) &= (1-r)(1-s) \\ N_2(r,s) &= r(1-s) \\ N_3(r,s) &= rs \\ N_4(r,s) &= (1-r)s \end{aligned} \tag{1}$$

The shape functions for nodes 5-8 are chosen as:

$$\begin{aligned} N_5(r,s) &= (1-s)P(r,\gamma) \\ N_6(r,s) &= rP(s,2) \\ N_7(r,s) &= sP(r,\gamma) \\ N_8(r,s) &= (1-r)P(s,2) \end{aligned} \tag{2}$$

where

$$P(x,\gamma) = 2\left(x - \frac{x^\gamma - 2(1/2)^\gamma x}{1 - 2(1/2)^\gamma} \right) \tag{3}$$

It can be easily shown that the shape functions for nodes 5-8 reduce to the standard quadratic serendipity element when γ of Equation (3) is set equal to 2. It can also be seen that the shape function for nodes 5-8 satisfies the interpolation property at all nodes of the element. That is:

$$N_i(r_j) = \delta_{ij} \quad \text{and} \quad N_i(s_j) = \delta_{ij}$$

where r_j and s_j are values of r and s at node j and δ_{ij} is the Kronecker delta. However, the shape functions associated with nodes 1-4 do not satisfy the interpolation property at nodes 5-8. Following the standard technique (Ref. 4), the shape functions for nodes 1-4 are modified as follows:

$$
\begin{aligned}
N_1 &\leftarrow N_1(r,s) - [N_8(r,s) + N_5(r,s)]/2 \\
N_2 &\leftarrow N_2(r,s) - [N_5(r,s) + N_6(r,s)]/2 \\
N_3 &\leftarrow N_3(r,s) - [N_6(r,s) + N_7(r,s)]/2 \\
N_4 &\leftarrow N_4(r,s) - [N_7(r,s) + N_8(r,s)]/2
\end{aligned}
\tag{4}
$$

where the $\leftarrow$ reads: "is replaced by."

It can now be seen that the shape functions for all eight nodes satisfy the required interpolation property. Additionally, the shape functions are capable of exactly representing the monomials $1, r, s, r^Y, rs, s^2, r^Y s$, and $s^2 r$. The presence of 1, r and s ensure representation of rigid body and constant strain modes. The presence of r^Y allows exact representation of displacements of the form r^Y. Note that this will result in a line singularity of the form r^{Y-1} upon differentiation.

In order to represent point singularities, the quadrilateral must be degenerated into a triangle. This is done by coalescing nodes 4, 8, and 1 as can be done for standard isoparametric elements (Ref. 5) and as is shown schematically in Figure 2. Thus, finally, for a point singularity, the shape function associated with node 1 is replaced with:

$$
N_1(r,s) \leftarrow N_1(r,s) + N_4(r,s) + N_8(r,s) \tag{5}
$$

This is easily programmed into the element routine. The generality of the above derivation allows use of the same shape functions as the basis of three-dimensional elements which possess line singularities.

In summary, for the 6 node triangle, the shape function associated with node 1 is given by Equation (5), the shape functions associated with nodes 2 and 3 are given by N_2 and N_3 of Equation (4), and the shape functions associated with nodes 5 through 7 are given by N_5 through N_7 of Equation (2).

Given the shape functions for the element, calculation of the stiffness matrix, thermal load vector, and gravity load vector follows the standard procedure as described in Reference 6. These quantities are therefore given as:

$$\underset{\sim}{K}^e = \int_{V^e} \underset{\sim}{B}^T \underset{\sim}{D} \underset{\sim}{B} \, dV$$

$$\underset{\sim}{F}^e_T = \int_{V^e} \underset{\sim}{B}^T \underset{\sim}{D} \underset{\sim}{\alpha} \Delta T \, dV \qquad (6)$$

$$\underset{\sim}{F}^e_b = \int_{V^e} \underset{\sim}{N}^T \underset{\sim}{b} \, dV$$

where

$$\underset{\sim}{B} = \underset{\sim}{L} \underset{\sim}{N} \quad , \quad \underset{\sim}{N} = [N_1 \underset{\sim}{I}, \; N_2 \underset{\sim}{I}, \; \ldots] \quad , \quad \underset{\sim}{L} = \begin{bmatrix} \frac{\partial}{\partial x} & 0 \\ 0 & \frac{\partial}{\partial y} \\ \frac{\partial}{\partial y} & \frac{\partial}{\partial x} \end{bmatrix} ,$$

and $\underset{\sim}{I}$ is a 2 × 2 identity matrix.

See Reference 6 for more details. The actual integration is performed via Gaussian quadrature. That is, the integrals are approximated as:

$$\int f(x) \, dx = \sum_{j=1}^{n} W_j \, f(a_j) \qquad (7)$$

Due to the formulation, it can be shown that along the s direction, the integration order needs to be, at most, 4 in order to exactly integrate the element. For an undistorted element, a maximum integration order of 3 is necessary, although often an integration order of 2 yields results just as good. Along the r direction, the method for an exact integration has not been ascertained. Currently, an integration order of 4 or 5 seems to suffice along the r direction. An exact integration formula analogous to the formula presented in Reference 3 or Reference 7 will hopefully be derived in the near future.

Calculation of the stress intensity factors are performed using the equations:

$$K_I = \frac{G}{2(1-\nu)} \lim_{r\to 0} \left(\frac{2\pi}{r}\right)^{1/2} u_y(\theta = \pi)$$

$$K_{II} = \frac{G}{2(1-\nu)} \lim_{r\to 0} \left(\frac{2\pi}{r}\right)^{1/2} u_x(\theta = \pi) \qquad (8)$$

where the nomenclature is shown in Figure 3. Alternatively, similar equations in terms of stresses can be used. It has been found here and noted elsewhere (Ref. 8) that Equation (8) yields more accurate results than the similar equations in terms of stresses. The values of the stress intensity factors are calculated at each of the integration points along the r direction and extrapolated to r=0 using Lagrangian interpolation.

Extension of the above formulation to three dimensions is straightforward. As discussed in Reference 4, the three-dimensional shape functions are simply products of the two-dimensional shape functions in r and s with the desired one-dimensional shape function in t. For example, the shape functions for the three-dimensional element of Figure 4 are given by:

$$N_1(r,s,t) = tN_1(r,s)$$
$$\vdots \qquad \vdots$$
$$N_6(r,s,t) = tN_6(r,s)$$
$$N_7(r,s,t) = (1-t)N_1(r,s)$$
$$\vdots \qquad \vdots$$
$$N_{12}(r,s,t) = (1-t)N_6(r,s)$$

The above element formulation may be extended to anisotropic materials by using the appropriate anisotropic material matrix D in Equation (6). When appropriate, D could be different at each integration point.

In order to incorporate plasticity effects, it is suggested that standard techniques currently used for plasticity in regular elements could also be applied to the present element. That is, after each load increment, each integration point in the element would be checked to see if it has gone plastic or not. If plasticity has occurred, then an algorithm such as radial-return (Ref. 9) would be used to bring the stress back to the yield surface. The element's internal forces, used to calculate the out-of-balance load vector would be given in standard form as:

$$\underset{\sim}{R}^e = \int_{V^e} \underset{\sim}{B}^T \underset{\sim}{\sigma} \, dV$$

Additionally, the order of the strain singularity would have to be updated, depending upon the hardening properties of the material (Ref. 10).

IMPLEMENTATION IN NASTRAN

Implementation of the crack element into NASTRAN was performed via the dummy element CDUM1. This procedure is covered in Reference 11. The present element was modeled after the QDMEM1 element routines, due to their similarity.

The first step was to create a subroutine KDUM1 which generates the stiffness and mass matrices. The mass matrix may be either consistent or lumped. When the mass matrix is used for calculation of gravity loads, the consistent mass matrix should be specified. This subroutine is eventually linked to NASTRAN LINK 8.

For computation of thermal loads, the subroutine EDTL must be modified to make a call to SSGETD before calling the routine DUM1. The dummy coding in routine DUM1 is then modified to calculate the thermal load vector based on the connecting grid point temperatures. Optionally, the element centroidal temperature could have been used, although this is generally not recommended since temperature gradients near the crack could not be accurately represented in this way. After modifying EDTL and DUM1, they must be linked to NASTRAN LINK 5.

Finally, the dummy coding for the SDUM11 and SDUM12 routines must be modified so that they perform the required operations. SDUM11 performs the preliminary geometry calculations and creates the S matrix which relates element stresses (including stress intensity factors) to the element's grid point displacements. SDUM12 then uses the S matrix, grid point displacements, and temperatures to compute the centroidal stresses and stress intensity factors and writes them to the output file. After modifying the SDUM11 and SDUM12 coding, it is linked to NASTRAN LINK 13. This completes the implementation into NASTRAN.

NUMERICAL RESULTS

In order to assess the accuracy of the present element, four different crack geometries/loading conditions with known solutions were analyzed. Figure 5 shows the different geometries analyzed. Figure 6 presents four different mesh sizes which were used to analyze the first three crack geometries. Figure 7 shows the boundary conditions used. For the edge crack with a point load, Figure 7 is modified so that the load is applied at the edge of the crack. Table 1 presents the errors associated with both the crack opening displacement (COD) and the mode I stress intensity factor K_I. As can be seen,

the COD is less sensitive to the mesh size, while the K_I values appear to be converging to their exact solutions. However, the edge crack with a point load solution appears to overshoot the exact by about 5%. It should be mentioned that the "exact" solution for the edge crack specimen with a point load is considered to be accurate to within 2%. The other exact solutions were considered to have accuracies better than 1%. These exact solutions were obtained from Reference 12.

Figure 8 presents a model of a central crack in a finite plate. To ascertain the accuracy of the element's mode II stress intensity factor, K_{II}, the model of Figure 8(a) was used. The results for both K_I and K_{II} are presented in Table 2. As can be seen, the K_{II} is within about 4% of the exact solution.

In summary, both COD and stress intensity factors appear to be accurately represented even for relatively course meshes. The accuracies obtained are well within the accuracies required by typical engineering calculations. This is due to the fact that the scatter alone, in the K_I values during a typical test, may be 10%.

CONCLUSIONS AND FUTURE RESEARCH

An element formulation has been presented that accurately models singularities. The form of the singularity is general and the two-dimensional element developed may be easily extended to three dimensions. Additionally, the element may be used as a standard, variable number of nodes quadratic element. The element has been incorporated into NASTRAN and compared to several known solutions.

Future research will include more tests of the element against known exact solutions. Additionally, an exact integration rule is desirable, and work to develop this will be performed. The element formulation will then be extended to three dimensions and the code will be incorporated into NASTRAN. Finally, extensions to include anisotropic materials and plasticity are possible and should be studied further.

REFERENCES

1. Barsoum, R. S., "On the Use of Isoparametric Finite Elements in Linear Fracture Mechanics," Int. J. for Numerical Methods in Engineering, Vol. 10, pp. 25-37, 1976.

2. Henshell, R. D. and Shaw, K. G., "Crack Tip Finite Elements are Unnecessary," Int. J. for Numerical Methods in Engineering, Vol. 9, pp. 495-507, 1975.

3. Stern, M., "Families of Consistent Conforming Elements with Singular Derivatives Fields," Int. J. for Numerical Methods in Engineering, Vol. 14, pp. 409-421, 1979.

4. Hughes, J. J. R. and Akin, J. E., "Techniques for Developing Special Finite Element Shape Functions with Particular Reference to Singularities," Int. J. for Numerical Methods in Engineering, Vol. 15, pp. 733-751, 1980.

5. Bathe, K. J. and Wilson, E. L., Numerical Methods in Finite Element Analysis, Prentice-Hall, 1976.

6. Zienkiewicz, O. C., The Finite Element Method, McGraw-Hill, 1977.

7. Dunham, R. S., "A Quadrature Rule for Conforming Quadratic Crack Tip Elements," Int. J. for Numerical Methods in Engineering, Vol. 14, pp. 287-312, 1979.

8. Parker, A. P., The Mechanics of Fracture and Fatigue, E.&F.N. Spon Ltd., London, 1981.

9. Krieg, R. D. and Key, S. W., "Implementation of a Time-Independent Plasticity Theory into Structural Computer Programs," in Constitutive Equations in Viscoplasticity: Computational and Engineering Aspects, J. A. Stricklin and K. J. Saczalski (eds.), ASME, New York, AMD Vol 20, pp. 125-137.

10. Hussian, M. A., Pu, S. L., and Lorensen, W. E., "Singular Plastic Element: NASTRAN Implementation and Application," Sixth NASTRAN Users' Colloquium, NASA Conference Publication 2018, 1977.

11. The NASTRAN Programmer's Manual, NASA SP-223(01), September 1972.

12. Tada, H., Paris, P. C., and Irwin, G. R., The Stress Analysis of Cracks Handbook, Del Research Corporation, Hellertown, Penn., 1973.

TABLE 1 ERRORS IN COD AND K_I AS A FUNCTION OF MESH

		37 Grid Mesh	77 Grid Mesh	86 Grid Mesh	95 Grid Mesh
CENTRAL CRACK	COD Error (%)	- 7.73	- 2.46	- 2.82	- 2.92
	K_I Error (%)	11.63	2.91	1.69	1.22
EDGE CRACK WITH UNIFORM STRESS	COD Error (%)	- 5.24	- 2.51	- 2.60	- 2.64
	K_I Error (%)	- 6.26	- 5.18	- 3.19	- 2.05
EDGE CRACK WITH POINT LOAD	COD Error (%)	-	-	-	-
	K_I Error (%)	-26.11	- 9.38	- 0.40	5.26

TABLE 2 ERRORS IN K_I and K_{II} FOR 234 GRID MESH

		Error (%)
CENTRAL CRACK IN SHEAR, FINITE PLATE	K_I	- 1.37
	K_{II}	4.23

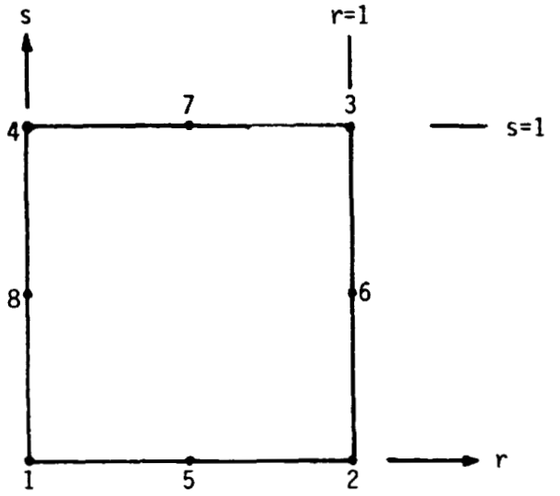

Figure 1 Nomenclature for Eight Node Isoparametric Element

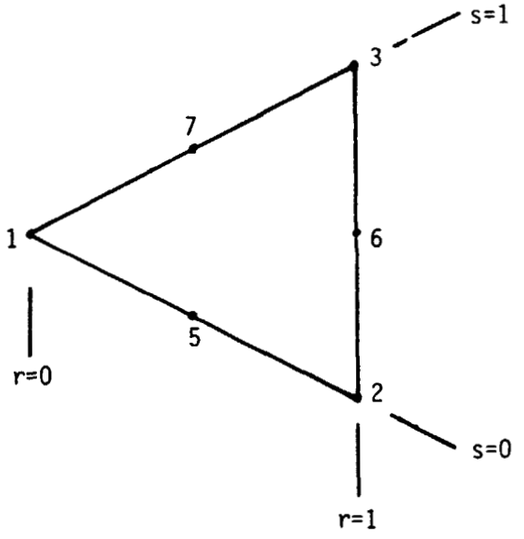

Figure 2 Degeneration of the Eight Node Element to a Six Node Triangular Element

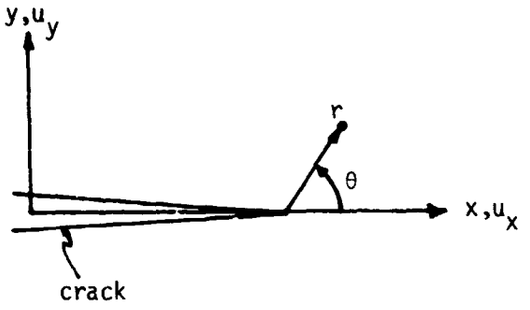

Figure 3 Nomenclature for Crack Geometry

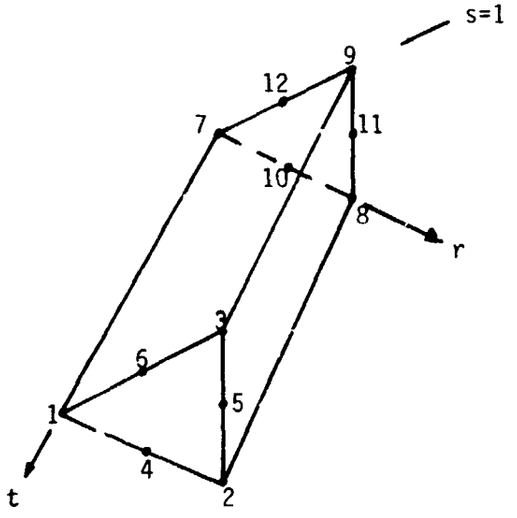

Figure 4 A Possible Three-Dimensional Generalization of the Two-Dimensional Element of Figure 2

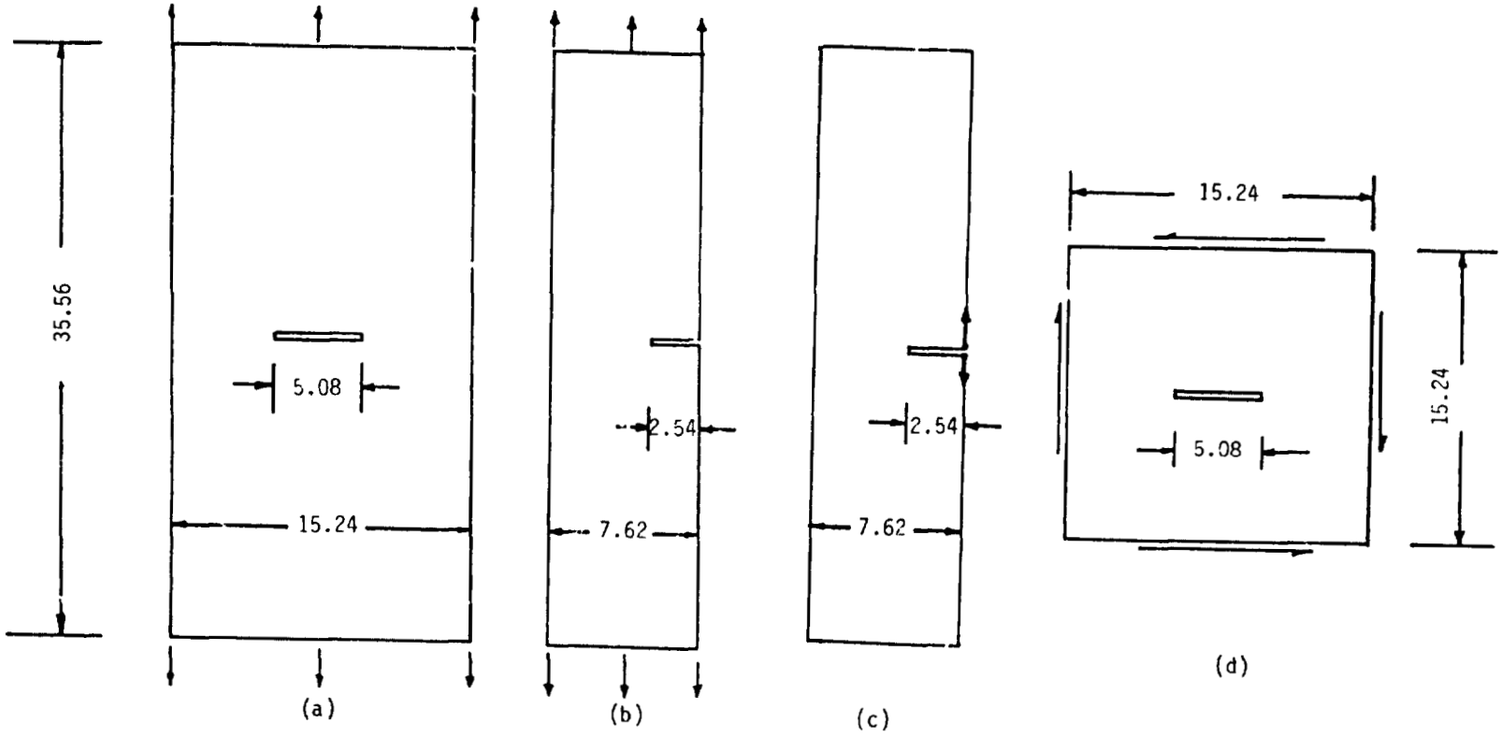

Figure 5 Crack Geometries Modeled (dimensions in cm's)
(a) central crack
(b) edge crack, uniform load
(c) edge crack, point load
(d) central crack in shear

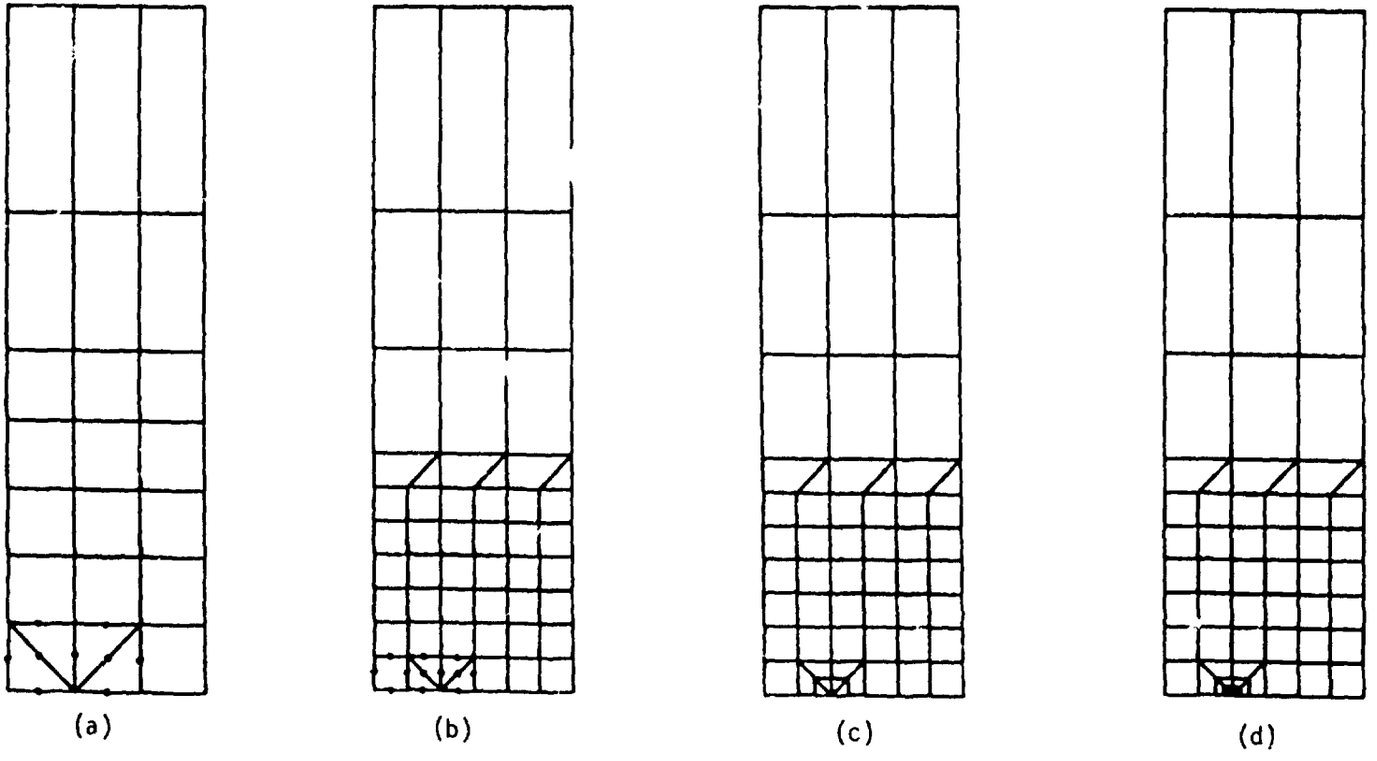

Figure 6 Different Mesh Sizes Analyzed
(a) 37 grid mesh
(b) 77 grid mesh
(c) 86 grid mesh
(d) 95 grid mesh

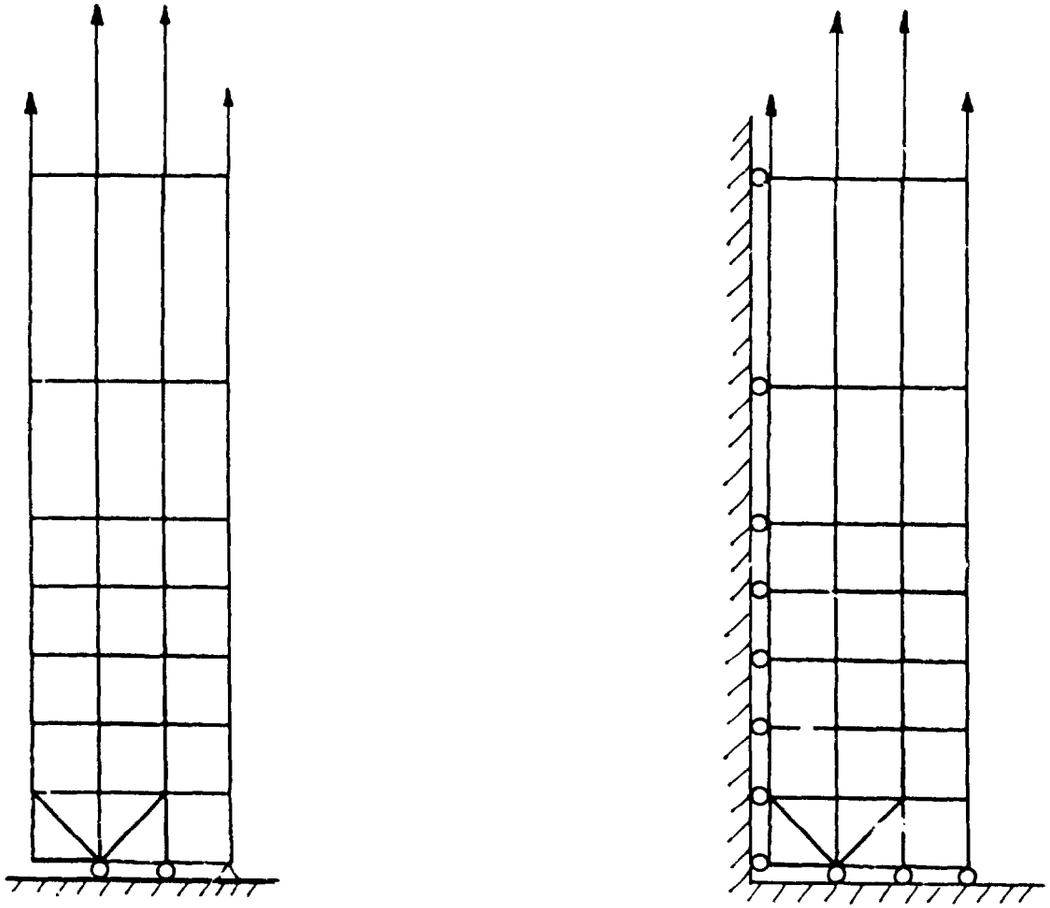

Figure 7 Boundary Conditions for Edge Crack and Central Crack Specimens
(a) edge crack
(b) central crack

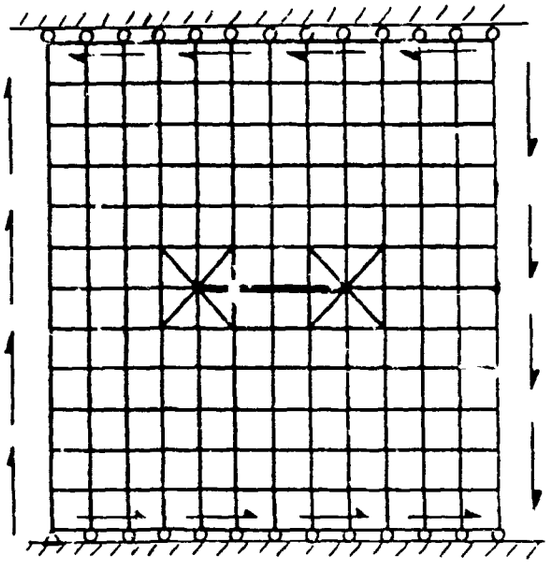

(a) loading condition for K_{II} calculation

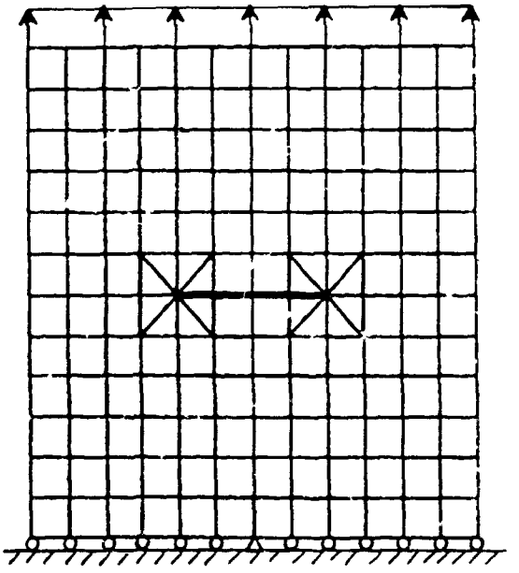

(b) loading condition for K_I calculation

Figure 8 Model of Central Crack in Finite Plate